

We report on high resolution spectra of the bright QSO HS 0747+4259 ($z_{\text{em}} = 1.90$, $V = 15.8$) observed to search for intermediate redshift O VI absorption systems. The spectra were obtained by means of the Space Telescope Imaging Spectrograph (STIS) at the Hubble Space Telescope (HST) and the High Resolution Echelle Spectrometer (HIRES) at the W. M. Keck telescope. We identify 16 O VI systems in the range $1.07 \leq z \leq 1.87$. Among them, six systems with $z_{\text{abs}} = 1.46 - 1.8$ exhibit a sufficient number of lines of different ionic transitions to estimate the shape of the ionizing radiation field in the range $1 \text{ Ryd} < E < 10 \text{ Ryd}$. All recovered UV ionizing spectra are characterized by the enhanced intensity at $E > 3 \text{ Ryd}$ compared to the model spectrum of Haardt & Madau (1996). This is in line with the observational evidence of a deficiency of strong Ly α absorbers with $N(\text{H I}) > 10^{15} \text{ cm}^{-2}$ at $z < 2$. The UV background shows significant local variations: the spectral shape estimated at $z = 1.59$ differs from that obtained at $z = 1.81$ and 1.73 . A possible cause of these variations is the presence of a QSO/AGN at $z \simeq 1.54 - 1.59$ close to the line of sight. No features favoring the input of stellar radiation to the ionizing background are detected, limiting the escape fraction of the galactic UV photons to $f_{\text{esc}} < 0.05$.

Key words. Cosmology: observations – Line: formation – Line: profiles – Galaxies: abundances – Quasars: absorption lines – Quasars: individual: HS 0747+4259

Spectral shape of the UV ionizing background and O VI absorbers at $z \sim 1.5$ towards HS 0747+4259^{*}

D. Reimers¹, I. I. Agafonova², S. A. Levshakov², H.-J. Hagen¹, C. Fechner¹, D. Tytler³, D. Kirkman³, and S. Lopez⁴

¹ Hamburger Sternwarte, Universität Hamburg, Gojenbergsweg 112, D-21029 Hamburg, Germany

² Department of Theoretical Astrophysics, Ioffe Physico-Technical Institute, 194021 St. Petersburg, Russia

³ Center for Astrophysics and Space Science, University of California, San Diego, MS 0424, La Jolla, CA 92093-0424, USA

⁴ Departamento de Astronomia, Universidad de Chile, Casilla 36-D, Santiago, Chile

received date; accepted date

Abstract.

1. Introduction

The ionization state of the intergalactic medium (IGM) is maintained by the metagalactic ionizing radiation field. The current paradigm considers the metagalactic UV field to be produced by the integrated radiation of QSOs reprocessed by the clumpy IGM (Haardt & Madau 1996, hereafter HM96; Fardal et al. 1998). Model calculations of the spectral energy distribution (SED) of the UV background depend crucially on the distribution of the Ly α forest lines – the number of absorption lines per unit redshift and per unit H I column density. This distribution is still poorly known. For instance, there is observational evidence suggesting a deficiency of strong absorbers with $N(\text{H I}) > 10^{15} \text{ cm}^{-2}$ at $z < 2$ compared to higher redshifts (e.g. Kim et al. 2001). These absorbers are the main source of the He II continuum opacity and their deficiency may result in a ionizing UV background much harder at energies $E > 4 \text{ Ryd}$ than model predictions based on biased absorber statistics (see HM96, Sect. 5.14). Another fact is that at $z < 2$ we observe significant spatial variations in the absorption line number density (Kim et al. 2002).

Closely related to the SED of the background ionizing radiation is the problem of a possible galactic (stellar) contribution. It is supposed that the emissivity of QSOs decreases dramatically at $z < 2$, whereas the input of galactic radiation to the ionizing background becomes more significant (e.g., Bianchi et al. 2001; Bolton et al. 2005). This conclusion is made from estimates of the mean intensity of the ionizing background at 912 Å. However, a putative galactic contribution would affect not only the intensity at the hydrogen ionization threshold but also the shape of the ionizing spectrum making it softer at $\lambda < 304$

Å (Leitherer et al. 1999; Giroux & Shull 1997). Thus, recovering the SED in the range $E > 4 \text{ Ryd}$ will enable us to estimate the relative contributions of QSOs and galaxies to the ultraviolet background.

To probe the shape of the ionizing radiation, optically thin absorption systems ($10^{13} \text{ cm}^{-2} \lesssim N(\text{H I}) < 10^{17} \text{ cm}^{-2}$) with metal lines can be used (Chaffee et al. 1986; Bergeron & Stasinska 1986). The ionization thresholds of ions usually observed in the intervening absorbers (Si II–Si IV, C II–C IV, N III, N V, O VI) lie between 1 and 10 Ryd and, thus, these boundaries limit the accessible energy range. Usually the shape of the ionizing continuum is estimated by a trial-and-error method. Recently we developed a special procedure based on techniques from the theory of experimental design that allows us to restore the SED directly from the analysis of absorbers with many metal lines (Reimers et al. 2005; Agafonova et al. 2005).

In this paper we report on the SEDs obtained from the analysis of metal absorbers with $z_{\text{abs}} = 1.46\text{--}1.81$ identified in the spectrum of HS 0747+4259. All absorbers studied reveal lines of O VI. This ion can be produced either collisionally in high temperature gas ($T_{\text{kin}} > 10^5 \text{ K}$) or by photoionization due to the background ionizing radiation. Particular interest in collisionally ionized O VI stems from the fact that O VI can trace the so-called ‘warm-hot intergalactic medium’ (WHIM) predicted in cosmological simulations (Cen & Ostriker 1999; Davé et al. 2001). Thus, the inferred shape of the ionizing continuum may help us to understand which mechanism is preferable for the interpretation of the observed O VI.

We also estimate the frequency of O VI absorbers in units of absorption distance, $\Delta\mathcal{N}_{\text{OVI}}/\Delta X$.

This paper is organized as follows. The observations are described in Sect. 2. Sect. 3 contains a short description of the computational methods used to analyze the absorption systems, which are studied in detail in Sect. 4. The results obtained are discussed and summarized in Sect. 5.

Send offprint requests to: S. A. Levshakov,
lev@astro.ioffe.rssi.ru

^{*} Based on observations obtained at the W. M. Keck Observatory and the HST

Table 1. Metal absorption-line systems toward HS 0747+4259

$z_1 = 1.9157$:	Ly α - δ ; C IV _{1548,1550} ; O IV ₇₈₇
$z_2 = 1.9070$:	Ly α - ϵ ; C IV _{1548,1550} ; O IV ₇₈₇
$z_3 = 1.8766$:	Ly α - ϵ ; C IV _{1548,1550} ; O IV ₇₈₇
$z_4 = 1.8617$:	Ly α - γ ; C IV _{1548,1550} ; O IV ₇₈₇ ; O VI ₁₀₃₁
$z_5 = 1.8533$:	Ly α - γ ; C IV _{1548,1550} ; O IV ₇₈₇ ; O VI ₁₀₃₁
$z_6 = 1.8073$:	Ly ₁₋₁₂ ; C II ₁₃₃₄ ; Si II ₁₂₆₀ ; C III ₉₇₇ ; O III ₈₃₂ ; Si III ₁₂₀₆ ; C IV _{1548,1550} ; O IV ₇₈₇ ; Si IV _{1393,1402} ; N V ₁₂₃₈ ; O VI _{1031,1037}
$z_7 = 1.7790$:	Ly α , β ; C IV _{1548,1550} ; O VI ₁₀₃₁
$z_8 = 1.7744$:	Ly α - ϵ ; C III ₉₇₇ ; C IV _{1548,1550} ; O IV ₇₈₇ ; O VI ₁₀₃₁
$z_9 = 1.7302$:	Ly ₁₋₈ ; C III ₉₇₇ ; Si III ₁₂₀₆ ; O III ₈₃₂ ; C IV _{1548,1550} ; O IV ₇₈₇ ; Si IV ₁₃₉₃ ; O VI _{1031,1037}
$z_{10} = 1.7154$:	Ly α - ϵ ; C IV ₁₅₄₈ ; O VI ₁₀₃₁
$z_{11} = 1.6331$:	Ly α - ϵ ; O III ₈₃₂ ; C IV _{1548,1550} ; O VI ₁₀₃₁
$z_{12} = 1.6134$:	Ly ₁₋₇ ; C III ₉₇₇ ; O III ₈₃₂ ; C IV _{1548,1550} ; O VI _{1031,1037}
$z_{13} = 1.5955$:	Ly ₁₋₇ ; C III ₉₇₇ ; O III ₈₃₂ ; Si III ₁₂₀₆ ; C IV _{1548,1550} ; Si IV ₁₃₉₃ ; O VI _{1031,1037}
$z_{14} = 1.5401$:	Ly β - γ ; C III ₉₇₇ ; C IV _{1548,1550} ; Si IV _{1393,1402} ; O VI _{1031,1037}
$z_{15} = 1.4856$:	Ly β ; C III ₉₇₇ ; C IV _{1548,1550} ; O VI ₁₀₃₁
$z_{16} = 1.4648$:	Ly β - ϵ ; C III ₉₇₇ ; C IV _{1548,1550} ; O VI _{1031,1037}
$z_{17} = 1.2910$:	Ly α - β ; C III ₉₇₇ ; C IV _{1548,1550} ; O VI ₁₀₃₁
$z_{18} = 1.1896$:	Ly α - β ; C III ₉₇₇ ; C IV _{1548,1550} ; O VI ₁₀₃₁
$z_{19} = 1.0778$:	Ly α ; C II ₁₃₃₄ ; Si II ₁₂₆₀ ; Si III ₁₂₀₆ ; Al III ₁₈₅₄ ; C IV _{1548,1550} ; Si IV _{1393,1402} ; O VI _{1031,1037}
$z_{20} = 1.0487$:	Ly α ; C IV _{1548,1550}
$z_{21} = 0.9277$:	Ly α ; Si II ₁₂₆₀ ; Si III ₁₂₀₆ ; Al III ₁₈₅₄
$z_{22} = 0.2616$:	Mg II _{2796,2803}
$z_{23} = 0.2237$:	Mg II _{2796,2803} ; Fe II ₂₆₀₀
$z_{24} = 0.2033$:	Mg II _{2796,2803} ; Fe II ₂₃₈₂
$z_{25} = 0.0$:	Mg I ₂₈₅₃ ; Mg II _{2796,2803} ; Ca II _{3934,3969} ; Mn II _{2594,2577} ; Fe II _{2600,2586,2382,2374,2344,2260}

Note: O VI $\lambda\lambda$ 1031, 1037 lines from systems with $z_{\text{abs}} > 1.8617$ fall in the gap between the HST/STIS and Keck/HIRES spectra

2. Observations

The UV spectrum of the quasar HS 0747+4259 ($z_{\text{em}} = 1.90$, $V = 15.8$; Reimers et al. 1998) was obtained with HST/STIS in September 2001 with a total exposure time of 54 180 seconds over 19 orbits. The spectrum was taken with the medium resolution NUV echelle (E230M) and $0.2'' \times 0.2''$ aperture, providing a resolution of $\lambda/\Delta\lambda \approx 30\,000$ (FWHM $\approx 10\text{ km s}^{-1}$). The spectrum covers the range from 2136 Å to 2970 Å. The data reduction was performed by the HST pipeline. After additional inter-order background correction, the 12 individual exposures were co-added. The resulting signal-to-noise S/N is 3-10 per pixel, lower than expected because the quasar was fainter by a factor of 2 in the UV compared to IUE observations (Reimers et al. 1998).

Another two integrations of HS 0747+4259 were obtained with HIRES on the Keck-I telescope: 3600 seconds on 2001 February 28, and 5400 seconds on 2001 March 01. The CCD was the single Tektronics engineering grade with 2048 by 2048 24 micron pixels that was fixed in HIRES from 1994 to mid-2004. Both integrations used a single setup covering 3060 Å to approximately 4560 Å with no gaps between the 39 spectral orders. We used the C5 dekker which contains a 1.148 arcsec wide slit hat gives high throughput and approximately 8 km s⁻¹ FWHM resolution. Before each integration of the QSO, 300 second integrations of the flux standard star G191 B2B were obtained. A Thorium-Argon lamp spectrum was used for the wavelength calibrations. The spectrum was extracted and reduced using Tom Barlow's MAKEE package, following procedures described in Kirkman et al. (2003) and

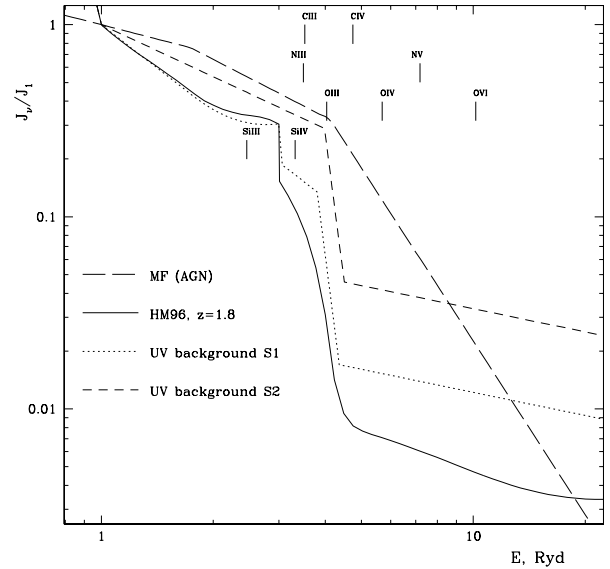


Fig. 2. Schematic picture of the $z = 2$ metagalactic (smooth line) and AGN-type (long-dashed line) ionizing backgrounds from Haardt & Madau (1996) and Mathews & Ferland (1987), respectively. The spectra are normalized so that $J_\nu(h\nu = 1\text{ Ryd}) = 1$. The positions of ionization thresholds of different ions are indicated by tick marks. The results of the restoring procedure are shown by the dotted (S1) and short-dashed lines (S2). For details, see text.

Suzuki et al. (2003). The obtained S/N declines systematically into the UV from ~ 30 at 4500 Å to ~ 5 below 3200 Å.

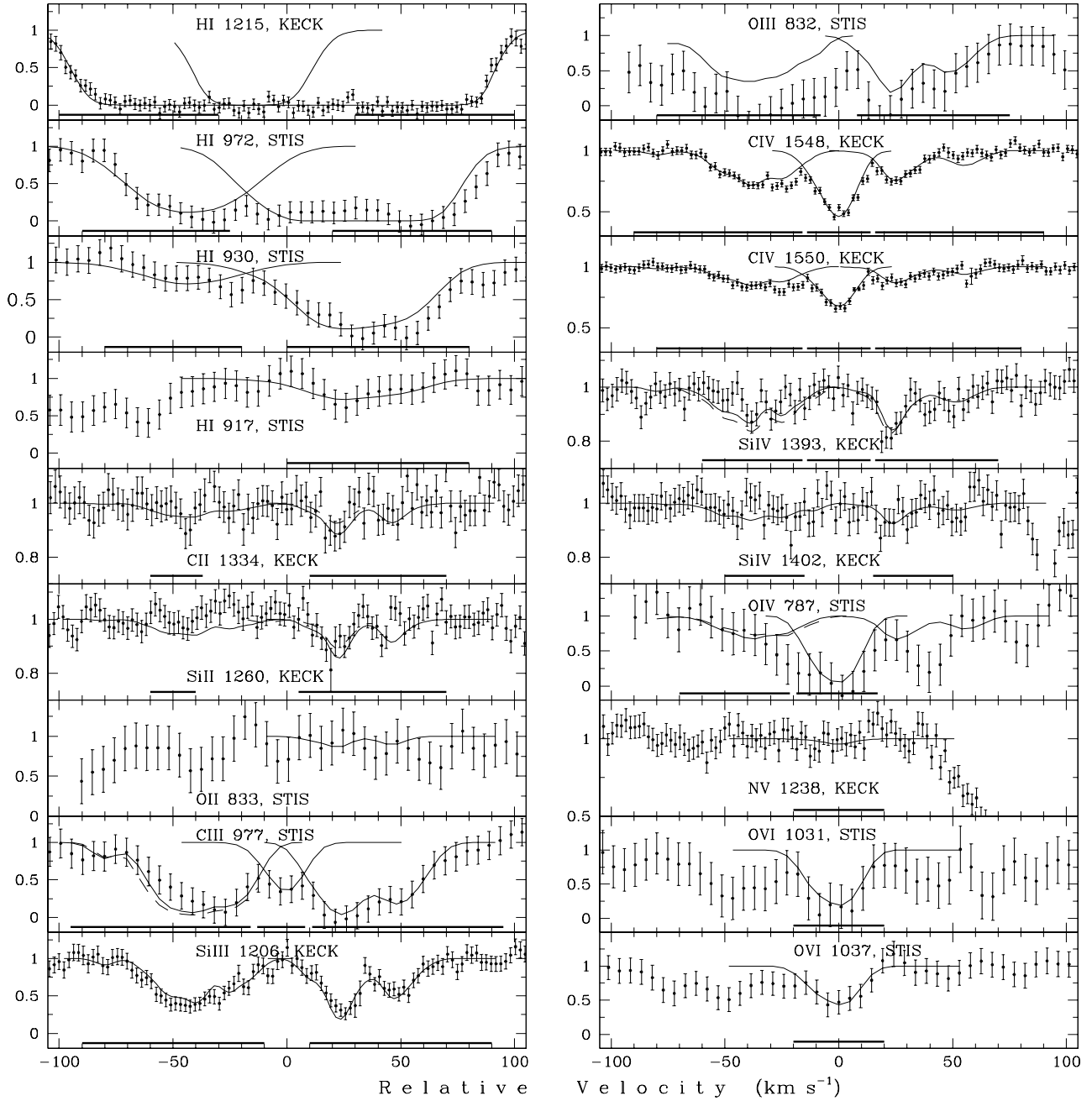


Fig. 1. Hydrogen and metal absorption lines associated with the $z_{\text{abs}} = 1.8073$ system toward HS 0747+4259. Continuum normalized intensities are shown by dots, along with 1σ error bars. The zero radial velocity is fixed at $z = 1.8073$. The smooth curves are synthetic spectra calculated with the ionizing background S1 (Fig. 2). The spectra are convolved with the corresponding spectrograph line-spread function. The physical parameters are listed in Table 2, Col.3, 5, and 6 (subsystems *A*, *B*, and *C*, respectively). The dashed lines show synthetic spectra computed with the HM96 ionizing spectrum (Fig. 2), the physical parameters are given in Cols.2 and 4, Table 2. Bold horizontal lines mark pixels included in the optimization procedure. The synthetic profiles of unmarked absorption lines were calculated in a second round using the velocity $v(x)$ and gas density $n_{\text{H}}(x)$ distributions already obtained in the optimization procedure.

3. Computational methods

The absorption systems are analyzed by means of the Monte Carlo Inversion (MCI) procedure described in detail in Levshakov, Agafonova & Kegel (2000, hereafter LAK), and with modifications described in Levshakov et al. (2002, 2003a,b). Here we briefly outline the basics needed to understand the results presented below in Sect. 4.

The MCI is based on the assumption that all lines observed in the absorption system are formed in a continuous medium where the gas density, $n_{\text{H}}(x)$, and velocity, $v(x)$, fluctuate from point to point (here x is the space coordinate along the line of sight).

Further assumptions are that within the absorber the metal abundances are constant, the gas is optically thin for the ion-

izing UV radiation, and the gas is in thermal and ionization equilibrium. This means that the fractional ionizations of all ions are determined exclusively by the gas density (or, equivalently, by the ionization parameter $U \propto 1/n_{\text{H}}$) and vary from point to point along the sightline. Since the ionization curves (i.e., the dependence of the ion fraction on U) are different for different ions, the ionic line profiles are different (non-similar) as well. Another important fact is that for a given point within the line profile the observed intensity results from a mixture of different ionization states due to irregular random shifts of the local absorption coefficient (see Fig. 1 in LAK).

The fractional ionizations are determined by the SED of the background ionizing radiation which is treated as an external parameter.

The radial velocity $v(x)$ and gas density $n_{\text{H}}(x)$ are considered as two continuous random functions which are represented by their sampled values at equally spaced intervals Δx . The computational procedure uses adaptive simulated annealing. The fractional ionizations of all elements included in the analysis are computed at every space coordinate x with the photoionization code CLOUDY (Ferland 1997).

In the MCI procedure the following physical parameters are directly estimated: the mean ionization parameter U_0 , the total hydrogen column density N_{H} , the line-of-sight velocity, σ_v , and density, σ_y , dispersions of the bulk material [$y \equiv n_{\text{H}}(x)/n_0$], and the chemical abundances Z_a of all elements involved in the analysis. With these parameters we can further calculate the column densities N_a for different species, and the mean kinetic temperature T_{kin} . The mean gas number density is related to the parameters of the gas cloud as [see eq.(28) in LAK]

$$n_0 = \frac{n_{\text{ph}}}{U_0} (1 + \sigma_y^2). \quad (1)$$

Here n_{ph} is the number density of photons with energies above 1 Ryd

$$n_{\text{ph}} = \frac{4\pi}{ch} J_{912} \int_{\nu_c}^{\infty} \left(\frac{J_{\nu}}{J_{912}} \right) \frac{d\nu}{\nu}, \quad (2)$$

where c , h , ν_c , and J_{ν} are the speed of light, the Planck constant, the frequency of the hydrogen Lyman edge, and the specific intensity (in $\text{ergs cm}^{-2} \text{ s}^{-1} \text{ sr}^{-1} \text{ Hz}^{-1}$). If the mean gas number density n_0 is known then the line-of-sight thickness L of the absorber can be evaluated as $L = N_{\text{H}}/n_0$.

An important issue in the analysis of the absorption systems is the treatment of unidentified blends which can affect the line profiles from the Ly α forest. Since the method supposes that all ions trace the same underlying gas density and velocity distributions, it is possible to reconstruct both distributions using the unblended parts of available lines. To clarify which parts may be blended several test runs with different arrangements of lines are carried out until a self-consistent fit for all lines observed in the system is found.

As mentioned above, the spectral shape of the ionizing radiation is treated as an external parameter: some standard ionizing spectrum is selected, corresponding ion fractions are calculated and then the MCI analysis is carried out with these fractions inserted. If the selected spectrum fails to reproduce

the observed line intensities or some other physical inconsistencies arise (e.g. odd element abundance ratios) the search for a more appropriate spectrum can be performed. The corresponding computational technique is described in Reimers et al. (2005) and Agafonova et al. (2005). It is based on the response surface methodology from the theory of experimental design and includes (i) the parameterization of the spectral shape by means of a set of variables (called ‘factors’), (ii) the choice of a quantitative measure (called the ‘response’) to evaluate the fitness of trial spectral shapes, and (iii) the estimation of a direction (in the factor space) which leads to a spectrum with better fitness. The optimal (best fitness) spectral shape is that which allows us to reproduce the observed intensities of all lines detected in the absorption system without any physical inconsistencies.

How well the spectral shape can be recovered depends on the number of metal lines involved in the analysis: the more lines of different ionic transitions of different elements are detected in the absorption system, the more constrained is the allowable set of shapes. When only a few lines are detected, they can be used to estimate the shape in some restricted energy interval. For example, lines of C III, C IV and O VI allow us in some cases to estimate the depth of the He II break ($E \geq 4$ Ryd). Any other a priori information concerning absorbers under study should be considered as well in order to distinguish between possible solutions.

4. Absorption systems towards HS 0747+4259

In the spectrum of HS 0747+4259 we identified over 50 absorption systems, among them 25 with metal lines (Table 1).

From these systems, only a few turned out to be suitable for analysis by MCI. The selection criteria included the presence of both lines in the C IV and O VI doublets, and at least one additional carbon line (e.g. C III) in order to fix the ionization parameter. As an initial guess for the UV background, the HM96 spectra at each corresponding redshift was used. The mean intensities of the ionizing background at $\lambda = 912 \text{ \AA}$, J_{912} , needed to calculate the number density of photons and the line-of-sight size of the absorbing gas, were also taken from HM96.

Note that these J_{912} values only slightly differ (within 20%) from those obtained from the proximity effect at $z = 1 - 2$ (Scott et al. 2002) and from measurements of the mean radiation flux transmitted through the Ly α forest (Tytler et al. 2004; Jena et al. 2005).

All computations below were performed with laboratory wavelengths and oscillator strengths taken from Morton (2003) for $\lambda > 912 \text{ \AA}$ and from Verner et al. (1994) for $\lambda < 912 \text{ \AA}$. Solar abundances were taken from Asplund et al. (2004).

The uncertainties of the physical parameter estimates (U_0 , N_{H} , σ_v , σ_y , and Z_a) are about 20%.

4.1. Absorption system at $z = 1.8073$

This complex absorption system containing lines of different ionic transitions is shown in Fig. 1. Unfortunately, some of these lines are corrupted by bad background subtraction and/or high noise (O III 832, O IV 788, probably also C III 977). Our

Table 2. Physical parameters of the $z_{\text{abs}} = 1.8073$ metal absorber towards HS 0747+4259 derived by the MCI procedure with the Haardt & Madau and modified UV background spectra (marked, respectively, by HM96 and S1 in Fig. 2). Column densities are given in cm^{-2}

Parameter ^a (1)	subsystem A $-90 \text{ km s}^{-1} < v < 0 \text{ km s}^{-1}$		subsystem B $0 \text{ km s}^{-1} < v < 80 \text{ km s}^{-1}$		subsystem C ^d $-20 \text{ km s}^{-1} < v < 20 \text{ km s}^{-1}$
	HM96	S1	HM96	S1	
	(2)	(3)	(4)	(5)	(6)
U_0	8.1E-3	4.5E-3	6.2E-3	4.1E-3	
N_{H}	1.2E18	7.7E17	7.6E18	4.7E18	
$\sigma_v, \text{ km s}^{-1}$	15.0	13.0	19.8	23.5	
σ_y	0.55	0.60	0.68	0.64	
Z_{C}	8.3E-5	1.0E-4	1.2E-5	1.7E-5	
Z_{O}	2.5E-4	3.6E-4	4.2E-5	6.0E-5	
Z_{Si}	1.1E-5	1.6E-5	1.8E-6	2.9E-6	
$[Z_{\text{C}}]$	-0.47	-0.37	-1.30	-1.15	
$[Z_{\text{O}}]$	-0.27	-0.10	-1.04	-0.90	
$[Z_{\text{Si}}]$	-0.46	-0.31	-1.25	-1.04	
$N(\text{H I})$	1.4E15	(1.4 ± 0.4)E15	1.0E16	(1.2 ± 0.3)E16	<3.0E14
$N(\text{C II})$	3.6E12 ^b	4.3E12 ^b	4.8E12	(7.0 ± 2.0)E12	...
$N(\text{O II})$	8.1E12 ^b	1.0E13 ^b	1.2E13 ^b	2.2E13 ^b	...
$N(\text{Si II})$	4.9E11 ^b	5.6E11 ^b	6.9E11	(9.0 ± 3.0)E11	...
$N(\text{C III})$	7.0E13	5.5E13 ^c	7.3E13	6.0E13 ^c	(1.0 ± 0.3)E13 ^e
$N(\text{O III})$	2.2E14	2.0E14 ^c	2.5E14	2.1E14 ^c	...
$N(\text{Si III})$	5.8E12	(6.1 ± 0.9)E12	8.4E12	(8.1 ± 1.2)E12	...
$N(\text{C IV})$	1.7E13	(1.50 ± 0.15)E13	1.1E13	(1.1 ± 0.1)E13	(1.9 ± 0.2)E13
$N(\text{O IV})$	5.6E13	(6.2 ± 2.0)E13	4.9E13 ^b	5.0E13 ^b	(2.9 ± 0.9)E14 ^e
$N(\text{Si IV})$	3.4E12	(2.6 ± 0.4)E12	2.2E12	(2.0 ± 0.4)E12	...
$N(\text{N V})$	≤2.0E12
$N(\text{O VI})$	(1.10 ± 0.25)E14
$\langle T \rangle, \text{ K}$	1.3E4	1.5E4	2.0E4	2.0E4	
$n_{\text{H}}, \text{ cm}^{-3}$	3.3E-3	6.6E-3	5.0E-3	7.6E-3	
$L, \text{ kpc}$	0.13	0.04	0.5	0.2	

^a $Z_{\text{X}} = N_{\text{X}}/N_{\text{H}}$; $[Z_{\text{X}}] = \log(N_{\text{X}}/N_{\text{H}}) - \log(N_{\text{X}}/N_{\text{H}})_{\odot}$; ^bcalculated using the velocity and density distributions estimated from the metal profiles marked by the horizontal bold lines in Fig. 1;

^cuncertainty cannot be estimated since line is corrupted by background subtraction;

^dcolumn densities for putative O VI absorption at $-70 \text{ km s}^{-1} < v < -20 \text{ km s}^{-1}$ and at $30 \text{ km s}^{-1} < v < 50 \text{ km s}^{-1}$ are not given because of probable blending with some Ly α forest lines (observed intensities of O VI $\lambda 1032$ and $\lambda 1037$ are inconsistent); ^ecan be blended

first computational runs revealed that the system consists of three subsystems with different physical parameters: low ionization subsystems at $-90 \text{ km s}^{-1} < v < 0 \text{ km s}^{-1}$ (subsystem A) and $0 \text{ km s}^{-1} < v < 80 \text{ km s}^{-1}$ (subsystem B) seen in C II-C IV, Si II-Si IV and O II-O IV and overlapping high ionization subsystem(s) seen in C IV and O VI at $-20 \text{ km s}^{-1} < v < 20 \text{ km s}^{-1}$ (subsystem C) and perhaps in O IV, O VI at $30 \text{ km s}^{-1} < v < 50 \text{ km s}^{-1}$ and in O VI at $-70 \text{ km s}^{-1} < v < -20 \text{ km s}^{-1}$.

In the following the subsystems A, B and C are treated separately. Calculations of subsystems A and B were carried out with the ionizing spectrum of HM96 at $z = 1.8$ (solid line in Fig. 2). The obtained physical parameters are given in Table 2, Col.2 and 4. Due to low S/N it was possible to reproduce almost all line profiles to within the noise level, i.e. the spectrum of HM96 may be considered as consistent with the ionization state of both subsystems. However, some overestimation of Si IV 1393 in the subsystem A and underestimation of C II 1334 and Si II 1260 in the subsystem B hint to probable inadequacy of the adopted spectral shape (Fig. 1, dashed lines). Low S/N

and bad background subtraction do not allow us to restore the SED of ionizing radiation via the directed search procedure described in Agafonova et al. (2005). However, the spectral shape can be probed by the ‘trial and error’ method. For example, the spectrum labeled as S1 in Fig. 2 delivers a better fit to the observed line intensities compared to HM96. The synthetic line profiles for the subsystems A and B calculated with physical parameters obtained with spectrum S1 (Col.3 and 5 in Table 2) are shown by the smooth lines in Fig. 2. Part of the C IV absorption at $-30 \text{ km s}^{-1} < v < 15 \text{ km s}^{-1}$ was not included in the calculations because of possible input from the subsystem C.

As for the highly ionized subsystem C, its hydrogen lines are hidden in the H I absorption lines of subsystem B. The upper limit for the H I column density along with the column densities for the C III 977, C IV 1548, 1550, O IV 832 and O VI 1031, 1037 lines identified in this subsystem (intensities at the expected positions of C III and O IV may be caused by unidentified blends) are given in Col.6 of Table 2. The FWHM of the O VI lines is 24 km s^{-1} which corresponds

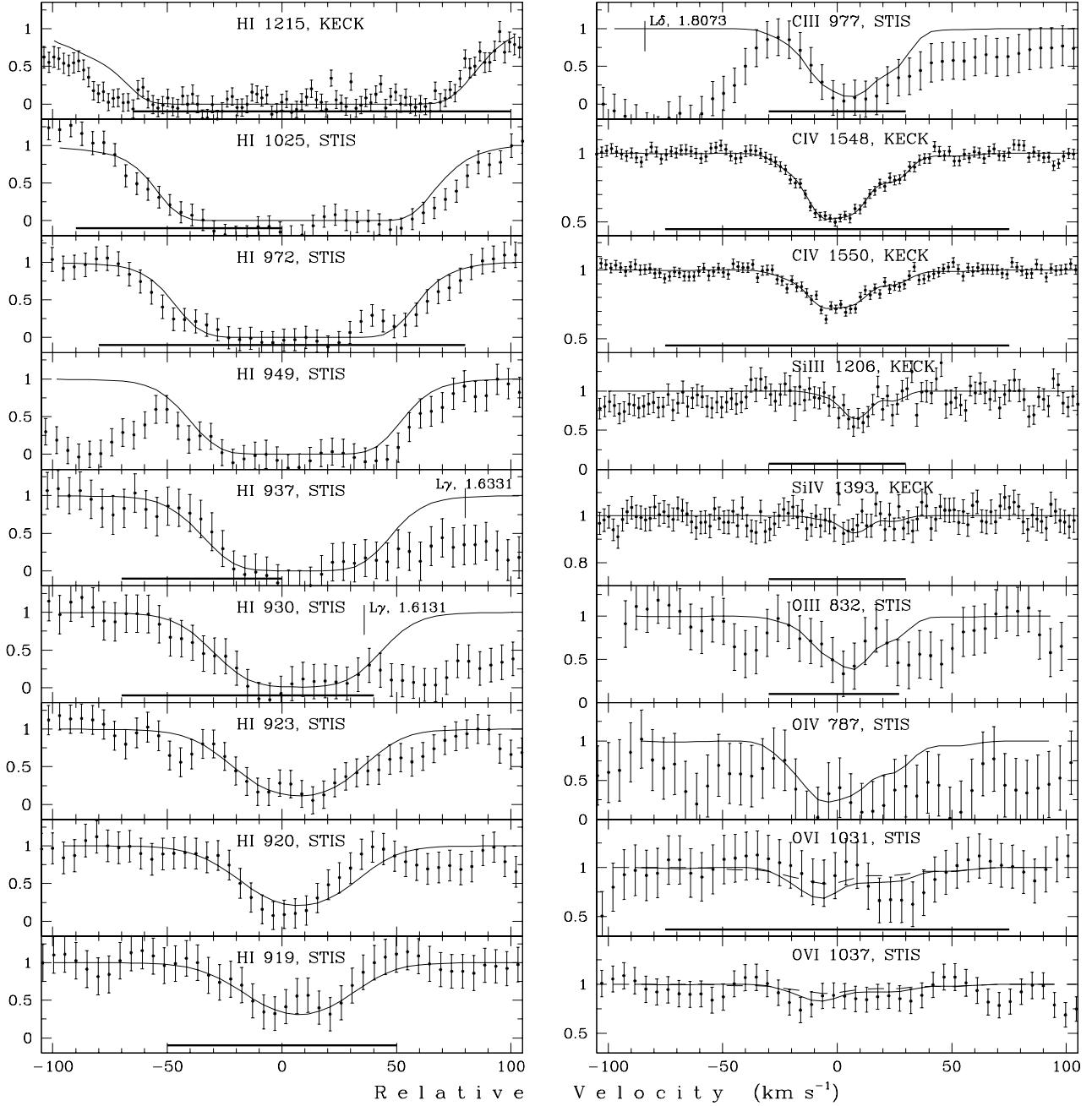


Fig. 3. Same as Fig. 1 but for the $z_{\text{abs}} = 1.7301$ system. The zero radial velocity is fixed at $z = 1.7301$. The physical parameters corresponding to the background S1 are listed in Table 3, Col.3, whereas those obtained with HM96 are in Table 3, Col.2. The central positions of blends are indicated by tick marks.

to $T_{\text{kin}} \sim 1.6 \times 10^5$ K if the line broadening is entirely thermal. According to Sutherland & Dopita (1993), maximal output of the O VI ion in the case of collisional ionization is reached at $T_{\text{kin}} = 3 \times 10^5$ K and decreases quickly at lower temperatures. Thus, this subsystem may be produced either by gas that has been (shock)-heated and is now cooling and recombining (non-equilibrium ionization) or by low-density gas in photoionization equilibrium with an ionizing background hard enough to account for the observed column density of O VI (e.g. such as HM96 or S1).

In general, the parameters obtained for the whole $z_{\text{abs}} = 1.8073$ absorption complex – high metallicity and low ionization compact clouds ($L \lesssim 0.2$ kpc) embedded in hot highly ionized gas – resemble gas observed in a burst out superbubble by Heckman et al. (2001). The suggested vicinity to a galaxy makes it interesting to test an ionizing background with significant input from stellar radiation, i.e. a spectrum which is softer at $E > 3$ Ryd compared to the QSO/AGN-dominated spectrum of HM96. The calculations show that any type of softer spectra can unambiguously be ruled out, since they poorly reproduce the observed line intensities and, moreover, lead to a relative

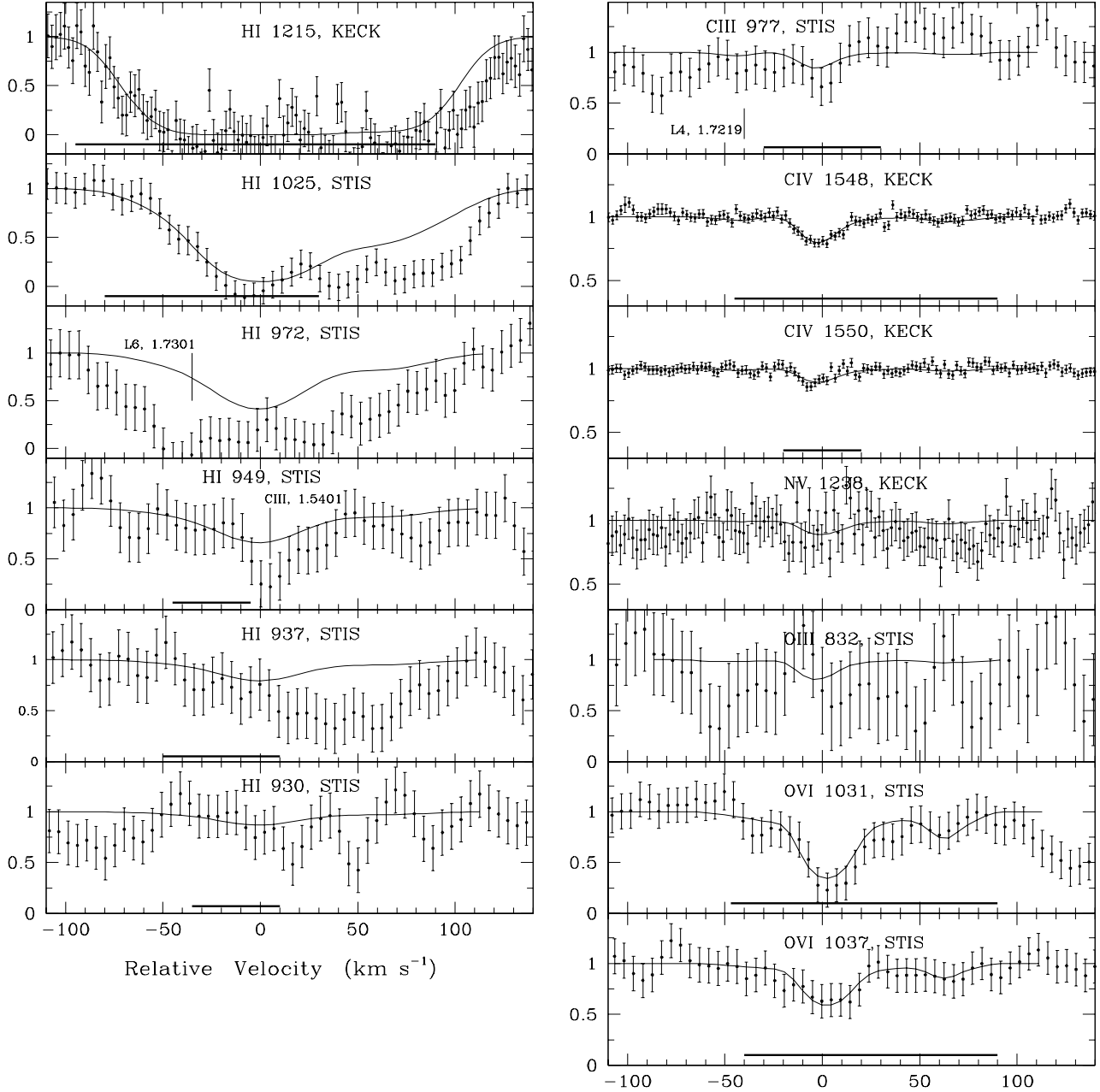


Fig. 4. Same as Fig. 1 but for the $z_{\text{abs}} = 1.6131$ system. The zero radial velocity is fixed at $z = 1.6131$. The physical parameters corresponding to the background S1 are listed in Table 3, Col.5, whereas those obtained with HM96 are in Table 3, Col.4. The central positions of blends are indicated by tick marks.

overabundance of carbon compared to silicon, ($[C/Si] > 0$). As far as we know, such an overabundance has never been measured in an H II region and is not expected theoretically.

4.2. Absorption system at $z_{\text{abs}} = 1.7301$

The system exhibits metal lines both in low (Si III 1206, O III 832) and high (C IV 1548, 1550; O VI 1032, 1037) ionization stages (Fig. 3). The parameters obtained from the MCI calculations with the HM96 spectrum are given in Col.2 of Table 3. With this ionizing background, the observed ratio of O III 832

and O VI 1032, 1037 lines is reproduced only marginally: a good fit to the O III line is accompanied by the underestimation of O VI (Fig. 3, dashed lines). Unfortunately, low S/N at the positions of these lines does not allow us to unambiguously reject the adopted spectrum. However, there is another inconsistency – the extremely large linear size of the absorber, $L \sim 200$ kpc. Linear sizes of this order of magnitude (hundreds of kpc) are expected for the filamentary large-scale structure, but the gas in the $z_{\text{abs}} = 1.7301$ system is too dense (number density $3 \times 10^{-4} \text{ cm}^{-3}$, overdensity $\delta_H \sim 80$) to be attributed to a filament. According to both observations (Chen et al. 1998, 2001)

Table 3. Physical parameters of the $z_{\text{abs}} = 1.7301$ and 1.6131 metal absorbers towards HS 0747+4259 derived by the MCI procedure with the Haardt & Madau and modified UV background spectra (marked, respectively, by HM96 and S1 in Fig. 2). Column densities are given in cm^{-2}

Parameter ^a	$z_{\text{abs}} = 1.7301$		$z_{\text{abs}} = 1.6131$	
	HM96	S1	HM96	S1
(1)	(2)	(3)	(4)	(5)
U_0	1.0E-1	5.7E-2	$\gtrsim 2.8\text{E}-1$	$\gtrsim 1.3\text{E}-1$
N_{H}	1.9E20	9.5E19	5.7E19	2.5E19
$\sigma_v, \text{km s}^{-1}$	24.9	24.5	26.4	24.5
σ_y	0.72	0.68	0.53	0.64
Z_{C}	8.1E-7	1.6E-6	3.1E-6	6.1E-6
Z_{N}	$< 2.0\text{E}-6$	$< 4.8\text{E}-6$
Z_{O}	2.8E-6	5.6E-6	1.8E-5	3.3E-5
Z_{Si}	1.4E-7	2.7E-7
$[Z_{\text{C}}]$	-2.50	-2.18	-1.90	-1.60
$[Z_{\text{N}}]$	< -1.5	< -1.1
$[Z_{\text{O}}]$	-2.24	-1.94	-1.41	-1.17
$[Z_{\text{Si}}]$	-2.37	-2.11
$N(\text{H I})$	1.9E16	$(1.9 \pm 0.4)\text{E}16$	7.3E14	$(7.2 \pm 2.0)\text{E}14$
$N(\text{C III})$	4.0E13	$(3.9 \pm 0.8)\text{E}13$	3.6E12	$(3.5 \pm 1.5)\text{E}12$
$N(\text{O III})$	1.3E14	$(1.3 \pm 0.4)\text{E}14$	3.9E13 ^b	3.0E13 ^b
$N(\text{Si III})$	1.7E12	$(1.7 \pm 0.2)\text{E}12$
$N(\text{C IV})$	3.1E13	$(3.10 \pm 0.15)\text{E}13$	1.2E13	$(1.1 \pm 0.1)\text{E}13$
$N(\text{O IV})$	2.3E14 ^b	2.4E14 ^b
$N(\text{Si IV})$	9.0E11	$(8.3 \pm 3.0)\text{E}11$
$N(\text{N V})$	$< 1.6\text{E}13$	$< 1.6\text{E}13$
$N(\text{O VI})$	2.8E13	$(4.0 \pm 1.0)\text{E}13$	1.3E14	$(1.30 \pm 0.25)\text{E}14$
$\langle T \rangle, \text{K}$	4.0E4	3.9E4	$\gtrsim 4.7\text{E}4$	$\gtrsim 4.5\text{E}4$
$n_{\text{H}}, \text{cm}^{-3}$	3.2E-4	5.6E-4	$\lesssim 1.0\text{E}-4$	$\lesssim 2.4\text{E}-4$
L, kpc	200	56	$\gtrsim 190$	$\gtrsim 35$

^a $Z_{\text{X}} = N_{\text{X}}/N_{\text{H}}$; $[Z_{\text{X}}] = \log(N_{\text{X}}/N_{\text{H}}) - \log(N_{\text{X}}/N_{\text{H}})_{\odot}$; ^b calculated using the corresponding velocity and density distributions estimated from the metal profiles marked by the horizontal bold lines in Figs. 3 and 4

and theoretical predictions (Davé et al. 1999), strong Ly α absorbers [$N(\text{H I}) > 10^{15} \text{ cm}^{-2}$] arise at impact parameters to a galaxy of $r < 50h^{-1} \text{ kpc}$. Thus, the linear size of the $z_{\text{abs}} = 1.7301$ absorber may be similar.

The ionizing spectrum of HM96 was modified in a way to enhance the O VI/O III ratio and to increase the gas number density [i.e. to decrease the mean ionization parameter U_0 , see eq.(1)]. The fractional abundance of O III decreases with the enhancement of the intensity at $3 < E < 4 \text{ Ryd}$ and the fraction of O VI becomes larger with higher intensity at $E > 4 \text{ Ryd}$. One of the acceptable spectral shapes is shown in Fig. 2 by the short-dashed line labeled as S1. Results obtained with S1 are given in Col.3 of Table 3, and the synthetic profiles are plotted in Fig. 3 by the smooth lines. Note that with the same normalizing intensity J_{912} the spectrum S1 gives nearly four times smaller linear size than the spectrum of HM96.

It should be stressed that the shape S1 is only one of the possible solutions for the $z_{\text{abs}} = 1.7301$ system since the low S/N of most of the spectral data allows us to vary the intensity at $E > 3 \text{ Ryd}$ over a broad range. Thus, the exact spectral shape cannot be recovered. Nevertheless, we can conclude that the absorption lines observed in this system favor spectra with increased intensity at $E > 3 \text{ Ryd}$ as compared to the HM96 model.

4.3. Absorption system at $z_{\text{abs}} = 1.6131$

This highly ionized system exhibits several hydrogen lines along with a weak C IV doublet and strong lines of O VI 1031, 1037 (Fig. 4). At the expected position of the Si IV 1393 line a clear continuum is present. The observed intensity at the position of the C III 977 line can be used only as an upper limit on the C III absorption since this line lies in a noisy part of the spectrum and is partly contaminated by Ly δ from the $z_{\text{abs}} = 1.7219$ system. This upper limit, along with a safe upper limit on the abundance ratio $[\text{O}/\text{C}] < 0.5$ known from measurements in Galactic and extragalactic H II regions and in metal poor halo stars (Henry et al. 2000; Akerman et al. 2004), are utilized to estimate the physical parameters in the absorber. The parameters obtained from the MCI calculations with the HM96 spectrum are listed in Col.4 of Table 3, whereas those obtained with the spectrum S1 (Fig. 2) are given in Col.5. The synthetic line profiles are identical in both cases and are shown by the smooth lines in Fig. 4.

The spectrum of HM96 leads to a linear size of hundreds of kpc and, hence, places the absorber in some filamentary structure. The spectrum S1 is harder at $E > 3 \text{ Ryd}$ and provides a line-of-sight size several times smaller, which allows us to attribute the absorber to a galactic halo.

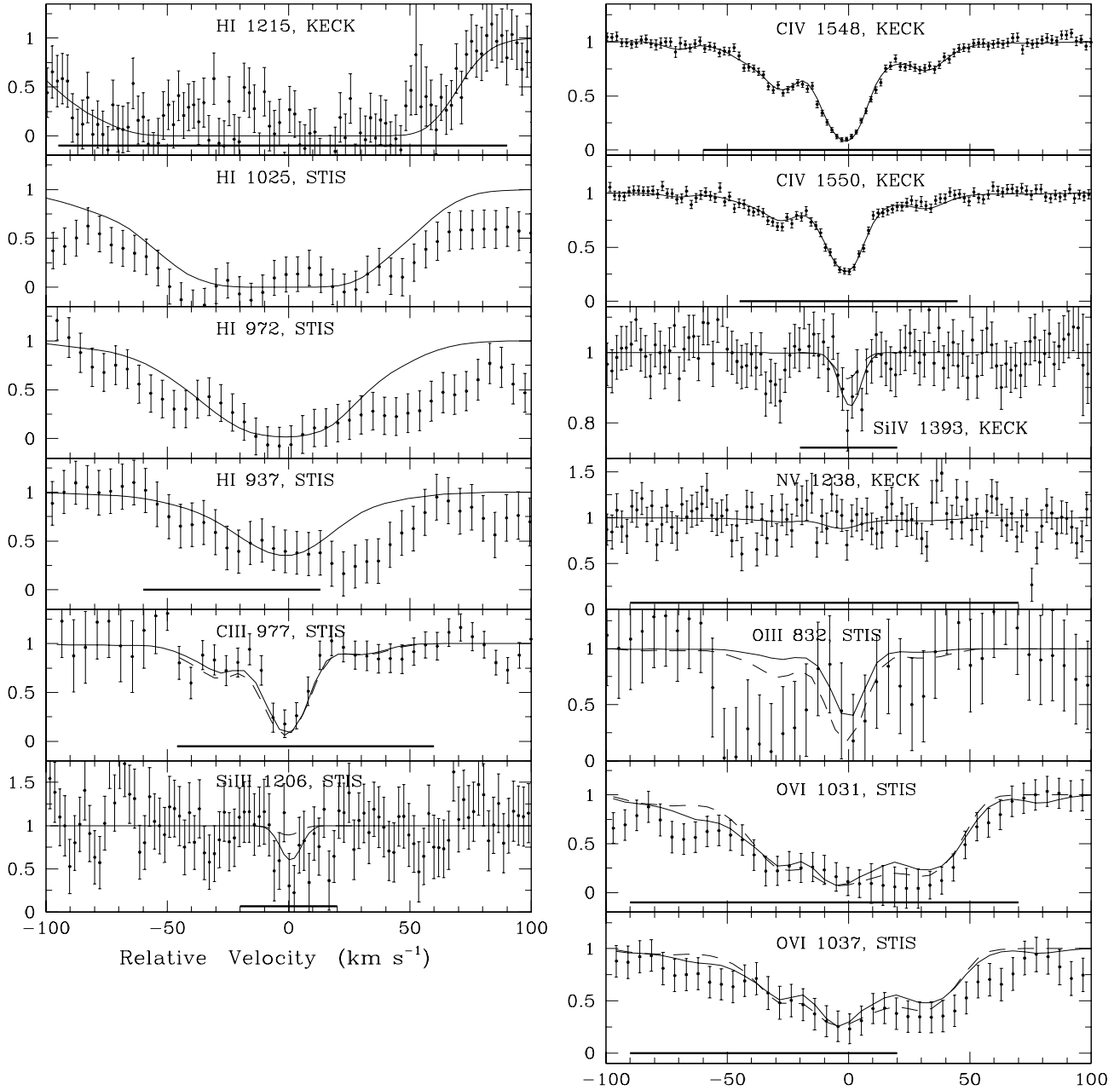


Fig. 5. Same as Fig. 1 but for the $z_{\text{abs}} = 1.5955$ system. Smooth curves are the synthetic spectra calculated with the ionizing background S2 (Fig. 2). The zero radial velocity is fixed at $z = 1.5955$. The physical parameters corresponding to the background S2 are listed in Table 4, Col.3, whereas those obtained with HM96 are in Table 4, Col. 2.

Both results are obtained assuming photoionization equilibrium for all observed ions. However, collisional ionization of O VI should be tested as well. From the apparent FWHMs of the available lines: H I (60 km s^{-1}), C IV (25 km s^{-1}), and O VI (35 km s^{-1}), and assuming pure thermal line broadening, we obtain kinetic temperatures of $T_{\text{HI}} = 7.6 \times 10^4 \text{ K}$, $T_{\text{CIV}} = 1.4 \times 10^5 \text{ K}$, and $T_{\text{OVI}} = 3.8 \times 10^5 \text{ K}$. Such diverse temperatures cannot occur in the same gas and thus turbulent broadening must be significant. The possibility of collisionally ionized O VI (with corresponding broad and shallow hydrogen lines hidden in the observed profile of H I) surrounds cooler gas producing H I and C IV absorption seems to be quite unprob-

able since the lines of C IV and O VI are well aligned in velocity space and have similar profiles. The case of non-equilibrium ionization can be ruled out as well since the recombination time of O VI is much shorter than that of hydrogen: for example, at $T_{\text{kin}} \sim 3 \times 10^5 \text{ K}$ it is about 60 times faster (Osterbrock 1974). Then the bulk of O VI should come to photoionization equilibrium prior to H I and we would observe a weak and shallow H I Ly α along with strong O VI lines. This contradicts the observed profiles in the $z_{\text{abs}} = 1.6131$ system. Therefore photoionization equilibrium is the most probable assumption.

It should be noted that O VI lines trace more rarefied gas not seen in C IV and, hence, can be broader. On the other hand, the

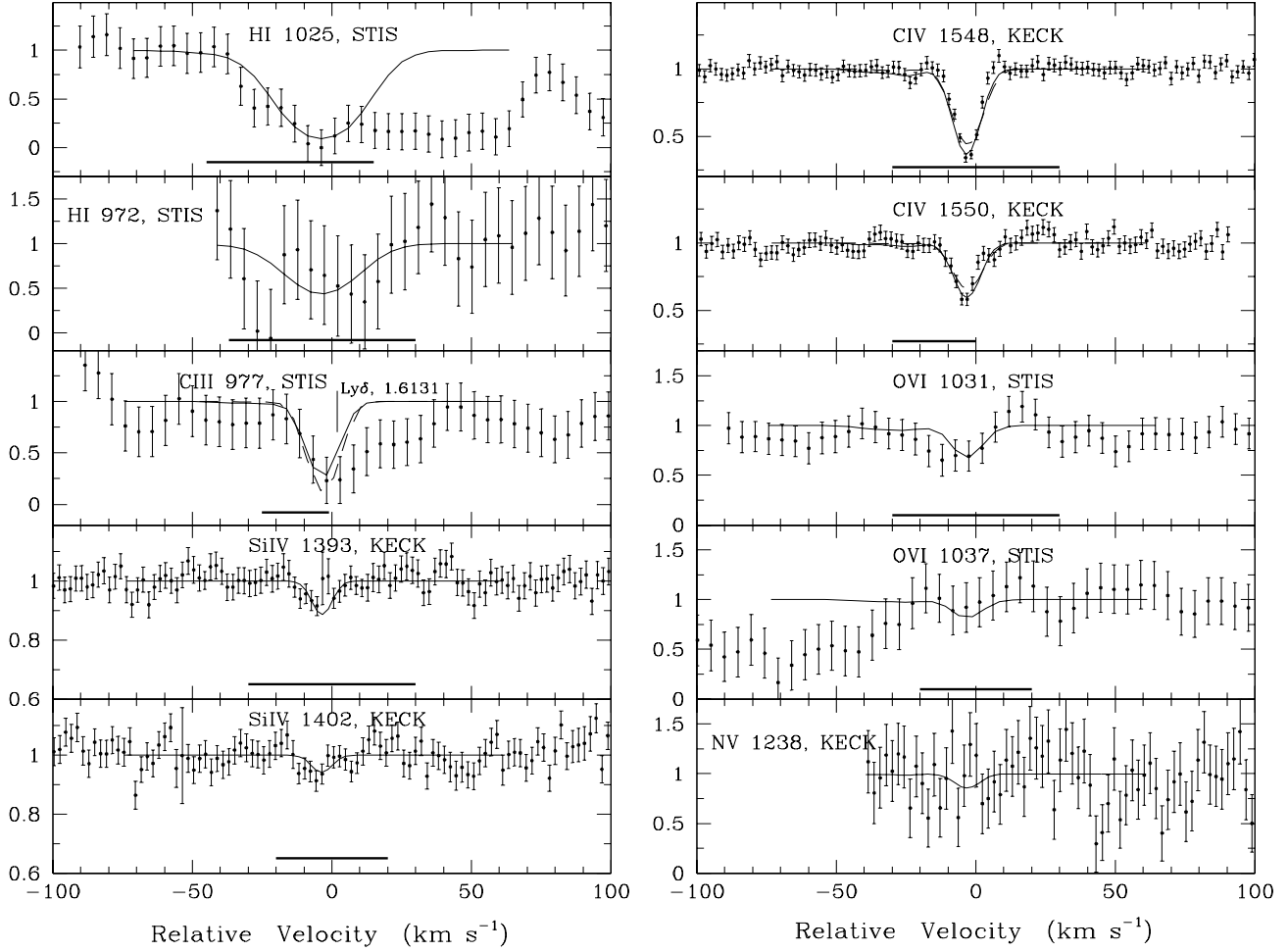


Fig. 6. Same as Fig. 1 but for the $z_{\text{abs}} = 1.5401$ system. The zero radial velocity is fixed at $z = 1.5401$. The smooth curves are the synthetic spectra calculated with the ionizing background S2 (Fig. 2). The physical parameters corresponding to the background S2 are listed in Table 4, Col.5, whereas those obtained with HM96 are in Table 4, Col.4. The central positions of blends are indicated by tick marks.

HI profile can be wider than O VI since some low density regions produce feeble O VI absorption not distinguishable from the noise. Thus, we can estimate the lower limit on the turbulent velocity dispersion from the comparison of the HI and O VI lines: $\sigma_{\text{turb}} > 19 \text{ km s}^{-1}$.

Taking into account such high turbulent velocities, the placement of the $z_{\text{abs}} = 1.6101$ absorber in a galactic halo, i.e. within boundaries where it remains gravitationally bound to a galaxy, seems to be more reasonable than its origin in the filamentary structure with no significant sources of the line broadening apart from the Hubble expansion. Thus, ionizing spectra that are harder at $E > 4 \text{ Ryd}$ as compared to that of HM96 are preferable for this absorber.

A few words should be said about the high upper limit on the nitrogen abundance since measurements usually show $[\text{N/C}] < -0.5$ for metal poor gas (Centurión et al. 2003). Unfortunately, the N V 1238 line in the absorber under study lies in a very noisy part of the Keck spectrum with many broad continuum undulations of unidentified nature. It is possible that this low contrast feature is not completely due to N V 1238 absorption.

4.4. Absorption system at $z_{\text{abs}} = 1.5955$

Absorption lines identified in this system are shown in Fig. 5. Note the very strong lines of O VI 1032, 1037 observed together with lines of Si III 1206 and Si IV 1393 (Si IV 1402 is blended). The physical parameters derived by the MCI assuming the HM96 ionizing background are listed in Col.2 of Table 4, and the corresponding synthetic profiles are shown by dashed lines in Fig. 5. This ionizing spectrum is not optimal: for the distribution of ionization parameters determined by the C III, C IV and O VI lines it significantly underproduces intensities of silicon lines (or, equivalently, delivers the ratio Si/O significantly higher than solar, which is inconsistent with measurements in H II regions) and it gives too large of a linear size. For this system non-equilibrium ionization can also be ruled out: the broadening of the C III 977, C IV 1548, 1550, O VI 1031, 1037 and hydrogen lines is similar. This points to significant contributions from turbulent velocities and, hence, to temperatures of about 10^4 K (see previous subsection). Moreover, there is a safe upper limit on the nitrogen abundance $[\text{N/C}] < -0.5$ obtained from the N V 1238 line: since N V traces the same gas

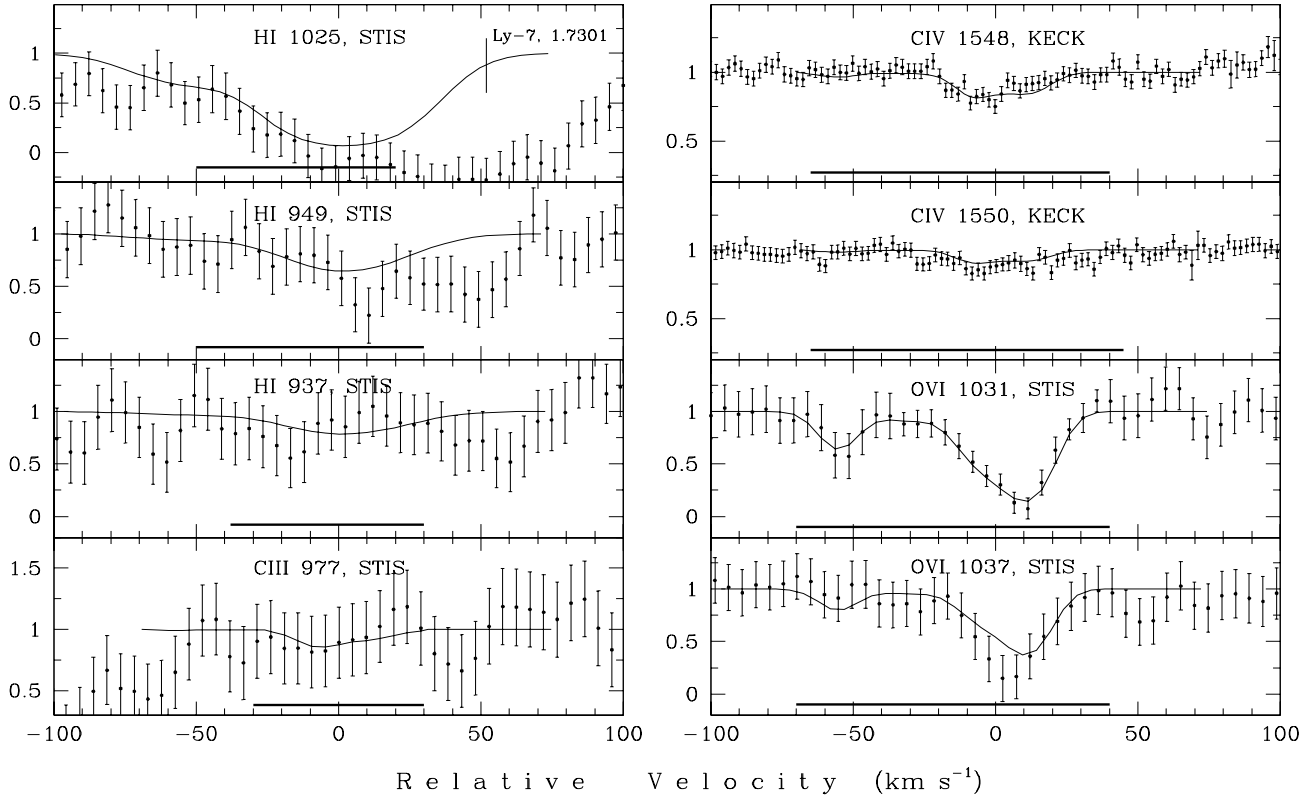


Fig. 7. Same as Fig. 1, but for the $z_{\text{abs}} = 1.4649$ system. The zero radial velocity is fixed at $z = 1.4649$. The physical parameters corresponding to the backgrounds HM96, S1, and S2 are listed in Table 4, Cols.6,7, and 8, respectively. The central positions of blends are indicated by tick marks.

as O VI, any ‘overionization’ of this gas would result in an artificial enhancement of the nitrogen abundance calculated under the assumption of equilibrium ionization. Thus, we look for a more appropriate ionizing background.

Taking into account information obtained with the HM96 spectrum and using the technique described in Reimers et al. (2005) and Agafonova et al. (2005), we searched for a background that would ensure a higher ratio of fractional ionizations $\Upsilon_{\text{SiIV}}/\Upsilon_{\text{CIV}}$ at the ionization parameter U determined from the C III, C IV and O VI absorption. Additionally, this U should be low enough to produce a physically reasonable linear size for the absorber under study. Other constraints to the solution were the inequalities $[\text{Si}, \text{O}/\text{C}] < 0.5$.

The resulting spectrum is shown in Fig.2 by the dashed line and marked as S2. It is significantly harder in the whole range $E > 1$ Ryd compared to both the initial spectrum of HM96 and the spectrum S1 used for the absorbers described in the preceding subsections. The physical parameters obtained from the MCI calculations with the S2 spectrum are listed in Col.3 of Table 4, and the corresponding synthetic profiles are plotted by the smooth lines in Fig. 5. Note that the derived element abundance ratios $[\text{Si}, \text{O}, \text{N}/\text{C}]$ are consistent with measurements in Galactic and extragalactic H II regions (e.g., Matteucci 2003).

The assortment and column densities of lines observed in the $z_{\text{abs}} = 1.5955$ system resemble those identified in some highly ionized high-velocity clouds (HVCs) at $z = 0$ (Collins

et al. 2004). Perhaps we are observing in the $z_{\text{abs}} = 1.5955$ absorber a high-redshift analog of the local HVCs.

One important difference between the spectra S2 and S1 should be emphasized. The shape S1 represents only one possible solution from a wide range of acceptable shapes since the low S/N for lines observed in the $z_{\text{abs}} = 1.8073$, 1.7301 and 1.6131 systems does not permit us to recover the SED with reasonable accuracy. Conversely, lines observed in the $z_{\text{abs}} = 1.5955$ system can be self-consistently described only with a quite narrow range of possible ionizing spectra and, hence, the spectrum S2 is determined much more accurately. In this context it is interesting to test the shape S2 on the absorption systems at $z_{\text{abs}} = 1.8073$ and 1.7301 exhibiting many metal lines. The result is negative – this spectral shape is inconsistent with line strengths observed in these systems. Thus, the ionizing radiation at $z < 2$ seems to undergo strong spectral variations.

4.5. Absorption system at $z_{\text{abs}} = 1.5401$

This absorption system is seen in H I Ly β and Ly γ and in metal lines shown in Fig. 6 (Ly α and Si III 1206 fall in the wavelength gap between the HST and Keck spectra). Note the unusually narrow C IV lines with $\text{FWHM} = 12.5 \text{ km s}^{-1}$.

The parameters derived from the MCI calculations with the HM96 ionizing spectrum are listed in Col.4 of Table 4. The synthetic profiles are shown in Fig. 6 by dashed lines. This spectrum is not completely consistent with the observed line in-

Table 4. Physical parameters of the $z_{\text{abs}} = 1.5955$, 1.5401 and 1.4649 metal absorbers towards HS 0747+4259 derived by the MCI procedure with the Haardt & Madau and modified UV background spectra (marked, respectively, by HM96, S1, and S2 in Fig. 2). Column densities are given in cm^{-2}

Parameter ^a (1)	$z_{\text{abs}}=1.5955$		$z_{\text{abs}}=1.5401$		$z_{\text{abs}}=1.4649$		
	HM96 (2)	S2 (3)	HM96 (4)	S2 (5)	HM96 (6)	S1 (7)	S2 (8)
U_0	2.4E-1	5.5E-2	1.8E-1	2.7E-2	$\gtrsim 3.4\text{E-1}$	$\gtrsim 1.8\text{E-1}$	$\gtrsim 8.8\text{E-2}$
N_{H}	1.0E20	1.6E19	2.2E18	4.7E17	6.8E19	2.6E19	1.3E19
$\sigma_v, \text{km s}^{-1}$	32.7	29.3	13.1	12.2	22.0	21.0	23.2
σ_y	0.64	0.60	0.83	0.41	0.46	0.60	0.35
Z_{C}	6.5E-6	4.4E-5	2.6E-5	1.5E-4	3.4E-6	6.8E-6	2.0E-5
Z_{N}	$< 4.5\text{E-7}$	$< 3.0\text{E-6}$	$< 1.1\text{E-5}$	$< 3.6\text{E-5}$
Z_{O}	3.2E-5	1.5E-4	7.4E-5	2.7E-4	1.8E-5	3.7E-5	6.0E-5
Z_{Si}	2.2E-6	7.6E-6	3.5E-6	1.8E-5
$[Z_{\text{C}}]$	-1.57	-0.74	-0.98	-0.21	-1.86	-1.55	-1.10
$[Z_{\text{N}}]$	< -2.1	< -1.3	< -0.74	< -0.2
$[Z_{\text{O}}]$	-1.15	-0.50	-0.80	-0.23	-1.40	-1.10	-0.90
$[Z_{\text{Si}}]$	-1.17	-0.63	-0.99	-0.26
$N(\text{H I})$	2.7E15	$(2.5 \pm 0.5)\text{E15}$	3.5E14	$(3.4 \pm 0.6)\text{E14}$	6.8E14	6.8E14	$(7.0 \pm 2.0)\text{E14}$
$N(\text{C III})$	3.8E13	$(3.6 \pm 0.6)\text{E13}$	1.6E13 ^b	1.3E13 ^b	2.6E12	2.6E12	$(1.8 \pm 0.9)\text{E12}$
$N(\text{O III})$	1.9E14 ^b	9.0E13 ^b
$N(\text{Si III})$	2.7E11	1.1E12
$N(\text{C IV})$	9.0E13	$(9.1 \pm 0.4)\text{E13}$	1.45E13	$(1.75 \pm 0.15)\text{E13}$	1.2E13	1.1E13	$(1.2 \pm 0.1)\text{E13}$
$N(\text{Si IV})$	5.2E11	$(1.00 \pm 0.15)\text{E12}$	6.1E11	$(5.9 \pm 0.6)\text{E11}$
$N(\text{N V})$	$< 7.5\text{E12}$	$< 9.5\text{E12}$	$< 4.0\text{E12}$	$< 4.0\text{E12}$
$N(\text{O VI})$	4.5E14	$(4.2 \pm 0.8)\text{E14}$	1.7E13	$(1.9 \pm 0.4)\text{E13}$	1.7E14	1.7E14	$(1.70 \pm 0.35)\text{E14}$
$\langle T \rangle, \text{K}$	3.5E4	3.0E4	2.8E4	2.0E4	$\gtrsim 4.8\text{E4}$	$\gtrsim 4.8\text{E4}$	$\gtrsim 3.3\text{E4}$
$n_{\text{H}}, \text{cm}^{-3}$	1.2E-4	5.1E-4	1.9E-4	1.2E-3	$\lesssim 6.7\text{E-5}$	$\lesssim 1.5\text{E-4}$	$\lesssim 3.0\text{E-4}$
L, kpc	280	10	4	0.13	$\gtrsim 280$	$\gtrsim 60$	$\gtrsim 15$

^a $Z_{\text{X}} = N_{\text{X}}/N_{\text{H}}$; $[Z_{\text{X}}] = \log(N_{\text{X}}/N_{\text{H}}) - \log(N_{\text{X}}/N_{\text{H}})_{\odot}$; ^b calculated using the velocity and density distributions estimated from the metal profiles marked by the horizontal bold lines in Fig. 5 ($z_{\text{abs}}=1.59$) and in Fig. 6 ($z_{\text{abs}}=1.54$)

tensities: it overestimates C III (the intensity of C III should be lower than the apparent intensity due to blending with Ly δ from the $z_{\text{abs}} = 1.6131$ system) and significantly underestimates the profiles of C IV 1548, 1550 in the center.

The spectra S1 and S2 were tried as well. S1 was rejected for the same reason as the spectrum of HM96 – poor reproduction of carbon lines. The spectrum S2 turned out to be consistent with the data. The physical parameters obtained with this background are listed in Col.5 of Table 4, and the corresponding synthetic line profiles are plotted in Fig. 6 (smooth lines).

This absorption system has characteristics which are quite unusual for intergalactic absorbers: metallicity of 0.6 solar and a sub-kiloparsec linear size. Probably it was ejected from a nearby galaxy located transverse to the line of sight. Note that the hard ionizing continuum derived for both $z_{\text{abs}} = 1.5955$ and $z_{\text{abs}} = 1.5401$ absorbers (separated by 6500 km s^{-1}) may be considered as a hint to the presence of an AGN in the vicinity of these systems (cf. S2 and the AGN-type spectrum of Mathews & Ferland in Fig. 2).

4.6. Absorption system at $z_{\text{abs}} = 1.4649$

This system is almost identical to that at $z_{\text{abs}} = 1.6131$ (the lines N V 1238, 1242 fall in the gap between Keck and STIS spectra). The physical parameters obtained from calculations

with the HM96, S1 and S2 spectra are listed in Col.6, 7 and 8 of Table 4, respectively. The synthetic profiles coincide for all three cases and are shown by the smooth lines in Fig. 7. The system exhibits a similar high turbulent velocity as found at $z_{\text{abs}} = 1.6131$. Therefore its origin in a filamentary structure is less favorable than an origin in a galactic halo and, hence, the harder spectra S1 and S2 are preferable to that of HM96.

4.7. Frequency distribution of O VI absorbers

The detection limit of O VI $\lambda 1302$ lines in the spectrum of HS 0747+4259 corresponds to $N(\text{O VI}) \gtrsim 2 \times 10^{13} \text{ cm}^{-2}$ ($W_{\text{rest}} \gtrsim 30 \text{ m\AA}$). In addition to the 6 absorbers described above, a further 10 metal systems in the redshift range 1.07 - 1.87 exhibit O VI $\lambda 1031$ absorption with the second line $\lambda 1037$ blended with Ly α forest absorption. However, the identification of O VI in these systems is certain due to the simultaneous detection of the C IV and O IV $\lambda 787$ lines (in absorbers with $z_{\text{abs}} > 1.7$). Table 5 lists the redshifts and column densities for the detected O IV lines.

With the absorption distance of $\Delta X = 1.27$ ($q_0 = 1/2$)¹, the number of encountered O VI absorbers translates into an absorber frequency of $\Delta \mathcal{N}_{\text{OVI}}/\Delta X = 13$. This is almost two

¹ $\Delta X = \frac{2}{3} [(1+z_1)^{3/2} - (1+z_2)^{3/2}]$

Table 5. O VI column densities

	z_{abs}	$N(\text{O VI}), \text{cm}^{-2}$	Comments
1	1.8617	$(3.2 \pm 0.8)\text{E13}$	$\lambda 1037$ blended
2	1.8533	$(3.0 \pm 0.8)\text{E13}$	$\lambda 1037$ blended
3	1.8073	$(1.1 \pm 0.3)\text{E14}$	
4	1.7790	$(2.5 \pm 0.8)\text{E13}$	$\lambda 1037$ below detection limit
5	1.7744	$(4.0 \pm 1.0)\text{E13}$	$\lambda 1037$ blended
6	1.7302	$(4.0 \pm 1.0)\text{E13}$	
7	1.7154	$(2.5 \pm 0.8)\text{E13}$	$\lambda 1037$ blended
8	1.6331	$(7.0 \pm 1.5)\text{E13}$	$\lambda 1037$ blended
9	1.6134	$(1.3 \pm 0.3)\text{E14}$	
10	1.5955	$(4.2 \pm 0.8)\text{E14}$	
11	1.5401	$(1.9 \pm 0.4)\text{E13}$	
12	1.4856	$(1.1 \pm 0.3)\text{E14}$	$\lambda 1037$ blended
13	1.4648	$(1.7 \pm 0.4)\text{E14}$	
14	1.2910	$(5.0 \pm 3.0)\text{E13}$	noisy spectrum, S/N ~ 3
15	1.1896	$(7.0 \pm 3.0)\text{E13}$	$\lambda 1037$ blended
16	1.0778	$(5.0 \pm 3.0)\text{E13}$	noisy spectrum, S/N ~ 3

times higher than $\Delta N_{\text{OVI}}/\Delta X = 7$ measured for the range $1.21 < z_{\text{abs}} < 1.67$ ($\Delta X = 0.72$) in the spectrum of HE 0515-4414 (Reimers et al. 2001). Thus, the O VI absorber statistics at $z_{\text{abs}} \sim 1.5$ is subject to strong variations from sightline to sightline. The mass density of the O VI absorbers, $\sum N(\text{O VI})/\Delta X$, shows even stronger variations: $(1.2 \pm 0.3) \times 10^{15} \text{ cm}^{-2}$ along the present sightline compared to $3.0 \times 10^{14} \text{ cm}^{-2}$ towards HE 0515-4414. Note, however, that the bulk of the integrated column densities in HS 0747+4259 comes from the strong O VI absorbers clustered at $1.46 < z_{\text{abs}} < 1.63$ where hard ionizing background was recovered. For comparison, at low redshift, $z \lesssim 0.15$, the O VI absorber frequency ($W_{\text{res}} > 30 \text{ mÅ}$) averaged over 31 FUSE sightlines is $\Delta N_{\text{OVI}}/\Delta X = 17 \pm 3$ (Danforth & Shull 2005). We recognize, however, such a comparison neglects the fact that the O VI systems at $z \sim 1.5$ are mainly photoionized, while those in the local universe may originate in the collisionally ionized intergalactic medium.

5. Conclusions

In this work, we investigate the O VI absorption line systems detected in the HST/STIS and Keck/HIRES spectra of the QSO HS 0747+4259. Six systems O VI with $z_{\text{abs}} = 1.46\text{--}1.81$ reveal a sufficient number of lines to perform a quantitative analysis of the shape of the UV background ionizing radiation. The results obtained lead to the following conclusions.

1. Spectral energy distributions with a significantly (> 2.5 times) higher intensity at $E > 4 \text{ Ryd}$ as compared to the model spectrum by HM96 are preferable for the absorption systems studied. Similar conclusion have been obtained in Agafonova et al. (2005) for the absorber at $z_{\text{abs}} = 1.9426$ towards J 2233-606. Such SEDs are suggested by the deficiency of strong Ly α absorbers [$N(\text{H I}) > 10^{15} \text{ cm}^{-2}$] at $z < 2$. On the other hand, the metagalactic SEDs obtained at $z \sim 3$ (Agafonova et al. 2005) show an intensity at $E > 4 \text{ Ryd}$ consistent with that of HM96. This confirms the conclusion of Kim et al. (2001) that absorbers with strong Ly α lines evolve faster than weak ones.

2. The spectral shapes recovered for the absorbers at $z_{\text{abs}} = 1.8073, 1.7301$ and at $z_{\text{abs}} = 1.5955, 1.5401$ are different with the latter being significantly harder in the whole range $E > 1 \text{ Ryd}$. There are theoretical predictions (Davé et al. 1999) that in general the evolution of the Ly α absorbers flattens at $z < 1.7$. However, this flattening would not lead to the increased ionizing flux. Thus, the observed variation of the spectral shape is probably of local nature and may be caused by the presence of a QSO/AGN close the line of sight (cf. Jakobsen et al. 2003).
3. The spectral shapes at $z < 2$ do not show signs of a significant contribution from galactic (stellar) radiation. According to Bianchi et al. (2001), an escape fraction $f_{\text{esc}} = 0.05$ results in a galactic contribution to the UV background at 912 Å equal to that of QSOs. Such galactic input would noticeably soften the ionizing spectrum in the range $E > 3 \text{ Ryd}$ (see, e.g., Giroux & Shull 1997). Taking into account the hardness of the recovered spectra at $E > 3 \text{ Ryd}$, the escape fraction of galactic photons at $z < 2$ should be well below 0.05. This is in line with $f_{\text{esc}} < 0.04$ estimated by Fernandez-Soto et al. (2003) from measurements of 27 galaxies with $1.9 < z < 3.5$.
4. In the systems considered, the main ionization mechanism for all observed ions including O VI is photoionization by the background UV radiation. The contribution of turbulence to the line broadening is significant and the temperatures estimated from the widths (FWHMs) of the O VI lines are well below the range where collisional ionization is dominant. High O VI column densities ($N > 10^{14} \text{ cm}^{-2}$) can originate in non-equilibrium gas which has been shock-heated and is now cooling and recombining (Heckman et al. 2002). Such conditions can be valid for very particular absorption system at $z_{\text{abs}} = 1.8073$ (subsystem C), but no other systems show signs of being non-equilibrial. Similar conclusions about the ionization of high redshift O VI are reported by Carswell et al. (2002), Bergeron et al. (2002), and Levshakov et al. (2003).

Acknowledgements. We thank staff of the W.M. Keck observatory, including instrument specialist Randy Cambell and observing assistants Gabrielle Saurage and Gary Puniwai. The work of I.I.A. and S.A.L. is supported by the RFBR grant 03-02-17522 and the RLSS grant 1115.2003.2. C.F. is supported by the Verbundforschung of the BMBF/DLR grant No. 50 OR 9911 1. D.T. and D.K. were supported in part by NASA StScI grant GO-9040.02 and by NSF grant AST-0098731.

References

- Agafonova, I. I., Centurión, M., Levshakov, S. A., & Molaro, P. 2005, A&A, in press (astro-ph/0506138)
- Akerman, C. J., Carigi, L., Nissen, P. E., Pettini, M., & Asplund, M. 2004, A&A, 414, 931
- Asplund, M., Grevesse, N., & Sauval, A. J. 2004, astro-ph/0410214
- Bergeron, J., & Stasinska, G. 1986, A&A, 169, 1
- Bergeron, J., Aracil, B., Petitjean, P., and Pichon, C. 2002, A&A, 396, L11
- Bianchi, S., Cristiani, S., & Kim, T.-S. 2001, A&A, 376, 1
- Bolton, J. S., Haehnelt, M. G., Viel, M., & Springel, V. 2005, MNRAS, 357, 1178

- Carswell, B., Schaye, J., & Kim, T.-S. 2002, *ApJ*, 578, 43
- Cen, R., & Ostriker, J. P. 1999, *ApJ*, 514, 1
- Chaffee, F.H., Jr., Foltz, C.B., Bechtold, J., & Weymann, R.J. 1986, *ApJ*, 301, 116
- Chen, H.-W., Lanzetta, K.M., Webb, J.K., & Barcons, X. 2001, *ApJ*, 559, 654
- Chen, H.-W., Lanzetta, K.M., Webb, J.K., & Barcons, X. 1998, *ApJ*, 498, 77
- Centurión, M., Molaro, P., Vladilo, G., Peroux, C., Levshakov, S. A., & D’Odorico, V. 2003, *A&A*, 403, 55
- Collins, J. A., Shull, J. M., and Giroux, M. L. 2004, *ApJ*, 605, 216
- Danforth, C. W., & Shull, J. M. 2005, *ApJ*, 624, 555
- Davé, R., Hernquist, L., Katz, N., & Weinberg, D. 1999, *ApJ*, 511, 521
- Davé, R., Cen, R., Ostriker, J. P. et al. 2001, *ApJ*, 552, 473
- Fan, X. et al. 2000, *AJ* 120, 1167
- Fardal, M. A., Giroux, M. L., & Shull, M. 1998, *AJ*, 115, 2206
- Ferland, G. J. 1997, *A Brief Introduction to Cloudy* (Internal Rep., Lexington: Univ. Kentucky)
- Fernandez-Soto, A., Lanzetta, K.M., & Chen, H.-W. 2003, *MNRAS*, 342, 1215
- Giroux, M. L., & Shull, J. M. 1997, *AJ*, 113, 1505
- Haardt, F., & Madau, P. 1996, *ApJ*, 461, 20 [HM96]
- Heckman, T. M., Norman, C. A., Strickland, D. K., & Sembach, K.R. 2002, *ApJ*, 577, 691
- Heckman, T. M., Sembach, K. R., Meurer, G. R. et al. 2001, *ApJ*, 554, 1021
- Henry, R. B. C., Edmunds, M. G., & Köppen, J. 2000, *ApJ*, 541, 660
- Jakobsen, P., Jansen, P. A., Wagner, S., & Reimers, D. 2003, *A&A*, 397, 891
- Jena, T., Norman, M.L., Tytler, D. et al. 2005, astro-ph/0412557
- Kim, T.-S., Carswell, R. F., Cristiani, S., D’Odorico, S., & Giallongo, E. 2002, *MNRAS*, 335, 555
- Kim, T.-S., Cristiani, S., and D’Odorico, S. 2001, *A&A*, 373, 757
- Kirkman, D., Tytler, D., Suzuki, N., O’Meara, J. M., & Lubin, D. 2003, *ApJS*, 149, 1
- Leitherer, C., Schaerer, D., Goldader, J. D. et al. 1999, *ApJS*, 123, 3
- Levshakov, S. A., Agafonova, I. I., Reimers, D., & Baade, R. 2003a, *A&A*, 404, 449
- Levshakov, S. A., Agafonova, I. I., D’Odorico, S., Wolfe, A. M., & Dessauges-Zavadsky, M. 2003b, *ApJ*, 582, 596
- Levshakov, S. A., Agafonova, I. I., Centurión, M., & Mazets, I. E. 2002, *A&A*, 383, 813
- Levshakov, S. A., Agafonova, I. I., & Kegel, W. H. 2000, *A&A*, 360, 833 [LAK]
- Matteucci, F., 2003, *The Chemical Evolution of the Galaxy* (Kluwer Academic Publishers:Dordrecht)
- Morton, D. C. 2003, *ApJS*, 149, 205
- Osterbrock, D. E. 1974, *Astrophysics of gaseous nebulae* (Freeman: San Francisco)
- Reimers, D., Janknecht, E., Fechner, C., Agafonova, I. I., Levshakov, S. A., & Lopez, S. 2005, *A&A*, 435, 17
- Reimers, D., Baade, R., Hagen, H.-J., & Lopez, S. 2001, *A&A*, 374, 871
- Reimers, D., Hagen, H.-J., Rodriguez-Pascual, P., & Wisotzki, L. 1998, *A&A*, 334, 96
- Shull, J. M., Tumlinson, J., Giroux, M. L., Kriss, G. A., & Reimers, D. 2004, *ApJ*, 600, 570
- Scott, J., Bechtold, J., Morita, M., Dobrzycki, A., & Kulkarni, V. P. 2002, *ApJ*, 571, 665
- Sutherland, R. S., & Dopita, M. A. 1993, *ApJS*, 88, 253
- Suzuki, N., Tytler, D., Kirkman, D., O’Meara, J. M., & Lubin, D. 2003, *PASP*, 115, 1050
- Tytler, D., Kirkman, D., O’Meara, J. et al. 2004, *ApJ*, 617, 1
- Verner, D. A., Barthel, P. D., & Tytler, D. 1994, *A&AS*, 108, 287
- Zheng, W., Kriss, G. A., Deharveng, J.-M., et al. 2004, *ApJ*, 605, 631